Finazzi, Vittoria; Monro, Tanya Mary; Richardson, David James.
Small-core silica holey fibers: nonlinearity and confinement loss trade-offs, *Journal of the Optical Society of America B - Optical Physics*, 2003; 20 (7):1427-1436.

Small-core silica holey fibers: nonlinearity and confinement loss trade-offs

Vittoria Finazzi, Tanya M. Monro, and David J. Richardson

Optoelectronics Research Centre, Southampton University, Southampton, SO17 1BJ, UK

Received July 31, 2002; revised manuscript received February 20, 2003

Holey fibers with small-core dimensions relative to the optical wavelength and large air-filling fractions offer tight mode confinement and are therefore attractive for highly nonlinear fiber applications. We investigated the role of confinement loss in these small-core fibers to optimize the design of practical highly nonlinear fibers. We found that silica holey fibers can exhibit effective nonlinearities as great as 52 W^{-1} km^{-1} and that the confinement loss can be less than the losses of standard fiber types. We show that the dispersive properties of some of the designs are suitable for a range of device applications. © 2003 Optical Society of America

OCIS codes: 060.4370, 060.2280, 060.2400.

1. INTRODUCTION

Nonlinear effects in fiber can be used for a wide range of optical processing applications in telecommunications and beyond. Examples include optical regeneration, wavelength conversion, optical demultiplexing, and Raman amplification. Consequently there is great interest in the development of fibers with high values of effective nonlinearity per unit length to reduce device lengths and the associated optical power requirements for fiber-based nonlinear optical devices. Even though silica is not intrinsically a highly nonlinear material, its nonlinear properties can be utilized in silica optical fibers if high intensities of light are guided within the core.[1]

A commonly used measure of the nonlinearity of a fiber is its effective nonlinearity γ,[1] given by

$$\gamma = \frac{2\pi}{\lambda}\frac{n_2}{A_{\text{eff}}}, \tag{1}$$

where n_2 is the nonlinear coefficient of the material, A_{eff} is the effective mode area, and λ the optical wavelength. For example, standard SMF28 fiber has an A_{eff} of $\sim$90 μm^2 at 1550 nm, and, as the n_2 of silica is $\sim 2.2 \times 10^{-20}$ m^2/W, γ is of the order of 1 W^{-1} km^{-1}. One way in which the nonlinearity of conventional silica fibers can be enhanced is to reduce the effective mode area by using a smaller core diameter and a higher index contrast [i.e., a larger numerical aperture (NA)]. Reference 2 showed that, by modifying the composition of a silica fiber and reducing the core diameter one can achieve values of γ as large as 20 W^{-1} km^{-1}. In this example, the addition of Ge to the fiber core increases n_2 to $\sim 5.4 \times 10^{-20}$ m^2/W and the NA to 0.37 and so reduces the effective mode area to $\sim$11 μm^2. With this enhanced NA and n_2, and assuming for simplicity a step-index fiber design, the largest γ that is possible is $\sim$26 W^{-1} km^{-1} (corresponding to a core diameter of 2.4 μm and an effective mode area of ~ 8 μm^2). To our knowledge, this result represents the largest NA and γ reported for a small-core conventional fiber. When even smaller core diameters are used, this NA becomes insufficient to confine the mode, and so the effective mode area increases, leading to smaller values of γ.

Silica holey fibers (HFs) can have significantly larger NAs than conventional silica fiber types because the cladding region can consist mostly of air. Holey fibers are a class of microstructured optical fibers in which the light is guided by means of average-index effects: the effective refractive index of the cladding region is lower than that of the solid silica core because of the presence of the holes. An example of such a fiber is shown in Fig. 1. Making use of the large NAs that are possible in these fibers, HFs can offer tighter mode confinement than conventional fibers. Hence HFs are attractive for nonlinear fiber devices.[3] Effective mode areas as small as $A_{\text{eff}} \sim 2.8$ μm^2 have been achieved at 1550 nm, corresponding to $\gamma \sim 35$ W^{-1} km^{-1} [Fig. 2(b)].[4] This is the best result in terms of nonlinearity in a silica fiber of which we are aware. In what follows, we show that pure silica HFs can be designed to have A_{eff} at least as small as 1.7 μm^2 at 1550 nm. Hence nonlinearities as high as $\gamma \sim 52$ W^{-1} km^{-1}, more than 50 times higher than in standard telecommunications fiber and 2 times higher than in the large-NA conventional fibers described above, are practical in these fibers.

Although these results indicate that HFs can dramatically enhance the achievable γ, the successful application of these fibers has been limited to date by loss, which is a consequence of the fact that these fibers are in an early stage of development. The losses in HFs occur for a variety of reasons: intrinsic material absorption, additional losses that arise during fabrication (water contamination, absorption owing to the presence of impurities, scattering, etc.), and confinement loss.[5] Fabrication-related losses can be reduced by careful optimization of the fabrication process, as was shown recently by researchers at the Nippon Telegraph & Telephone Company[6] (NTT), who reported a loss of 1 dB/km. This represents the lowest loss known at this time in a HF. Confinement loss is an additional form of loss that occurs in single-material fibers. In single-material HFs the core

0740-3224/2003/071427-10$15.00

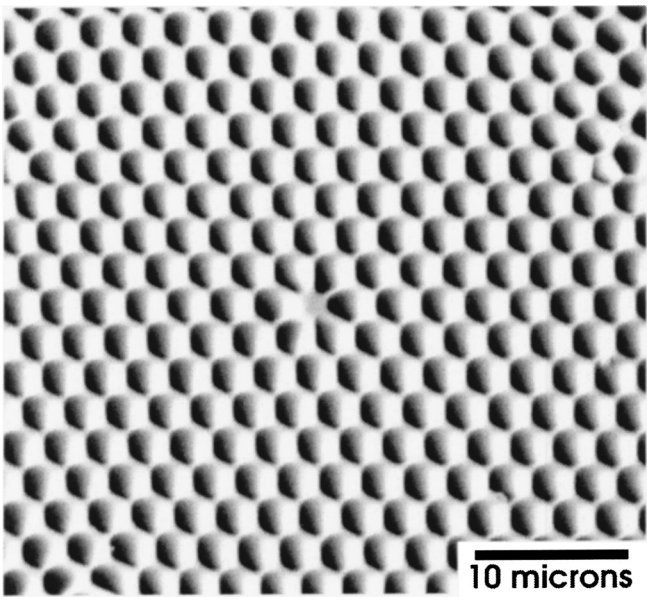

Fig. 1. Typical small-core silica holey fiber with 12 rings of regularly spaced air holes (only the central region is shown).

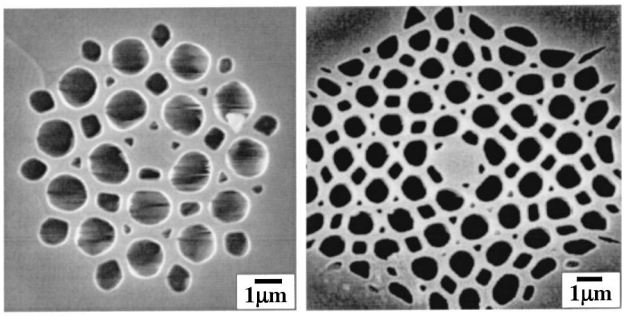

Fig. 2. Small-core holey fibers with (a) two rings of large air holes, and (b) four rings of large air holes.

has the same refractive index as the material beyond the finite holey cladding region, so every propagating mode is therefore intrinsically leaky. It has been proved that increasing the number of rings of air holes that surround the solid core, and thereby increasing the physical separation between the solid core and the external environment, reduces confinement loss.[5] Thus confinement loss is determined by the geometry of the structure, and we show that it can contribute significantly to the loss for these fibers unless care is taken with the fiber design.

We recently predicted that confinement loss will contribute significantly to the loss of HFs when the core dimensions are reduced.[7] The losses so far measured in real small-core HFs are typically of the order 50 dB/km,[8] more than an order of magnitude larger than the best loss achieved at NTT for a larger core design. Figures 2(a) and 2(b) show two small-core fibers with similar effective mode areas ($A_{\text{eff}} = 2.6\ \mu\text{m}^2$ and $A_{\text{eff}} = 2.8\ \mu\text{m}^2$ at 1550 nm, respectively). The fiber shown in Fig. 2(a) has a cladding that comprises two rings of large air holes, and the measured loss is 1 dB/m at 1550 nm. The fiber in Fig. 2(b), made by the same fabrication procedure but with the number of rings of large holes increased to four, has a measured loss of 0.04 dB/m. Inasmuch as it is reasonable to assume that both fibers suffer similar absorption and scattering losses, we conclude that increasing the number of rings in the small-core regime has served to reduce the fiber loss by improving the confinement of the mode. Thus confinement loss can significantly contribute to the total loss for these fibers. Note that the structural irregularities do not contribute significantly to the loss for the fibers shown here.

To make the fiber fabrication process practical, we ideally wish to limit the number of rings that are required. It is therefore important to be able to calculate reliably the confinement loss characteristics for these HFs. In this paper we identify the fiber designs that produce low-loss highly nonlinear fibers. Note that although fiber loss limits the effective length of any nonlinear device, for highly nonlinear fibers, short lengths (<10 m) are typically required, so loss values of the order of 1 dB/km can be readily tolerated.

2. MODEL

Using the multipole method developed in Refs. 5 and 9 has allowed us to calculate the confinement loss within a variety of structures. This technique was applied to two classes of microstructured optical fiber, both index-guiding HFs[5] and photonic bandgap fibers.[9] The multipole method is a scattering technique, implemented as a full-vector modal approach so it can accurately represent the large refractive-index contrast that is present in microstructured optical fibers. Here we outline the basics of the approach only; for a more detailed explanation of the method, see Ref. 9. The method can be applied to any microstructured optical fiber with a cladding region defined by a finite number (N_c) of circular holes of arbitrary refractive index (here we consider air holes only) that are embedded in a uniform material (here taken to be silica glass). The cladding region is enclosed within a circular jacket of arbitrary refractive index. Here an absorbing jacket is used; the real part of the refractive index is taken to be that of silica, and the imaginary part is taken to be small. According to the multipole approach, the boundary of each hole in the microstructured optical fiber is effectively a source of radiating fields that is due to fields transmitted through the boundary from sources beyond it and to fields reflected from the boundary itself.

The jacket was introduced for a number of reasons. Mathematically, it ensures the square integrability of the fields on the transverse plane. In addition, using a complex refractive index for the jacket allows the confinement loss to be estimated because the jacket absorbs the portion of the mode that leaks. Note that the result of the calculation is insensitive to the choice of jacket radius and to its imaginary refractive index. In what follows, $\mathbf{r} = (r, \theta)$ is the polar coordinate system of the jacket.

Given the circular geometry of the holes, cylindrical harmonic functions centered on each hole can be used to describe the field. In the proximity of the lth air hole, we express the longitudinal electric field in terms of Bessel (J_m) and Hankel [$H_m^{(1)}$] functions, using the local cylindrical coordinate centered at $\mathbf{c}_l$ (position of the hole), resulting in the following local expansion[9]:

$$E_z(\mathbf{r}, z) = \sum_{m=-\infty}^{\infty} [A_m^{El} J_m(k_\perp^e|\mathbf{r} - \mathbf{c}_l|) + B_m^{El} H_m^{(1)}(k_\perp^e|\mathbf{r} - \mathbf{c}_l|)]\exp\{\mathrm{im}[\arg(\mathbf{r} - \mathbf{c}_l)]\}\exp(i\beta z), \quad (2)$$

where $k_\perp^e$ is the transverse wave-vector component in the host glass material and the superscript El of coefficients A_m and B_m corresponds to the electric field of the lth hole. The J_m terms are bounded everywhere and represent the part of field E_z incident upon a cylinder that comes from all the other cylinders, whereas the diverging $H_m^{(1)}$ terms represent the part of the field that is propagating away from the cylinder boundary. A similar expansion can be written for the jacket, with superscript 0 instead of l. The local expansion [Eq. (2)] for each hole is valid in an annular region centered on the hole and extending to the perimeter of the nearest air hole.

To describe the field throughout the host material we need to introduce a global expansion. According to Wijngaard,[10] the field at any point within a material can be represented as superposition of outgoing waves from all source bodies within the material[9]:

$$E_z(\mathbf{r}, z) = \sum_{l=1}^{N_c} \sum_{m=-\infty}^{\infty} B_m^{El} H_m^{(1)}(k_\perp^e|\mathbf{r} - \mathbf{c}_l|) \times \exp\{im[\arg(\mathbf{r} - \mathbf{c}_l)]\}\exp(i\beta z) + \sum_{m=-\infty}^{\infty} A_m^{E0} J_m(k_\perp^e r)\exp(im\theta)\exp(i\beta z). \quad (3)$$

This global expansion is valid throughout the host material. Expansion (3) contains outgoing waves from each cylinder (l) and a standing-wave term generated at the jacket boundary (superscript 0). The longitudinal component of the magnetic field is expanded by use of the same approach as for the electric field but with different expansion coefficients (superscript H instead of E).

For consistency, the local expansion for the field in the vicinity of each cylinder needs to be equated with the global expansion. The resultant equation involves terms related to the transforms between the local and the global coordinate systems and can be solved by use of Graf's addition theorem.[11] This theorem can readily be applied to any arbitrary nonoverlapping arrangement of circular holes.

Next, it is necessary to combine the contributions from all the cylinders. To build up a consistent description of the electric and magnetic fields from the local description related to the different cylinders, we apply both the boundary conditions and the Rayleigh identity.[12] The boundary conditions require the continuity of the tangential electric and magnetic field components at the boundary of each cylinder and of the jacket. They can conveniently be written in terms of reflection coefficients, producing a reflection matrix $\mathcal{R}$ for all the cylinders and $\tilde{\mathbf{R}}^0$ for the jacket.[9] The Rayleigh identity requires that the J_m (incident) parts of the field near cylinder l ($\mathbf{A}^{El} = [A_m^{El}]$) be due to the $H_m^{(1)}$ fields radiated ($\mathbf{B}^{Ei} = [B_m^{Ei}]$) from all the other cylinders ($i \neq l$). This field radiated from the other cylinders can arrive either directly on cylinder l or by backreflection with the jacket ($\mathbf{A}^{E0} = [A_m^{E0}]$). This relation is again determined by use of Graf's addition theorem.

Following this procedure, we can consistently relate initial field expansions (2) and (3), resulting in a unique field identity that depends only on the coefficients B_m^{El} and B_m^{Kl}. These unknown coefficients can be written as a vector $\mathcal{B} = [\tilde{\mathbf{B}}^l]$, where $\tilde{\mathbf{B}}^l = [\mathbf{B}^{El^{\mathrm{T}}}\ \mathbf{B}^{Kl^{\mathrm{T}}}]^{\mathrm{T}}$ and the superscript T denotes the transpose. After some manipulations,[9] the field identity becomes the following infinite homogeneous linear system of algebraic equations:

$$\mathcal{M}\mathcal{B} \equiv [\mathbf{I} - \mathcal{R}(\tilde{\mathcal{H}} + \tilde{\mathcal{J}}^{B0}\tilde{\mathbf{R}}^0\tilde{\mathcal{J}}^{0B})]\mathcal{B} = 0, \quad (4)$$

where $\mathbf{I}$ is the identity matrix and $\tilde{\mathcal{H}}$, $\tilde{\mathcal{J}}^{0B}$, and $\tilde{\mathcal{J}}^{B0}$ are translation matrices that express the change of basis transformations considered above. Note that the $\tilde{\mathcal{H}}$ term in $\mathcal{M}$ describes direct cylinder-to-cylinder interactions, whereas $\tilde{\mathcal{J}}^{B0}\tilde{\mathbf{R}}^0\tilde{\mathcal{J}}^{0B}$ describes all indirect interactions between cylinders that take place by means of reflections ($\tilde{\mathbf{R}}^0$) at the jacket boundary.

For a given geometry, matrix $\mathcal{M}$ contains just one unknown, the mode propagation constant β. The propagation constant is related to the effective index of the propagating mode n_{eff} by $\beta = (2\pi/\lambda)n_{\mathrm{eff}}$. By inspection, Eq. (4) indicates that nontrivial solutions occur when the determinant of matrix $\mathcal{M}$ is zero (i.e., when $\mathcal{M}$ is singular). This method yields the complex effective index, and thus the confinement losses can be calculated as follows:

$$\text{confinement loss } [\mathrm{dB/m}] = \frac{20 \times 10^6}{\ln 10} \frac{2\pi}{\lambda\ [\mu\mathrm{m}]} \mathrm{Im}(n_{\mathrm{eff}}). \quad (5)$$

The use of a polar coordinate system centered in every hole allows the symmetry properties of the structure to be accurately described. The idealized structures considered within this paper consist of hexagonally packed rings of holes. According to group theory,[13] this kind of structure belongs to the C_{6v} symmetry group (6-fold rotational symmetry with at least one reflection plane) and so supports nondegenerate and 2-fold degenerate modes only. In addition, idealized 6-fold symmetric fiber profiles are not birefringent.[14] All these fiber characteristics are preserved by the model.[14] Moreover, the use of local polar coordinate systems makes this approach efficient.[5]

After finding values of β that result in $\mathcal{M}$ being singular, we evaluate the null space vector(s) $\mathcal{B}$ corresponding to this solution by performing a singular value decomposition. Note that not all solutions correspond to physical solutions for the fiber modes. Inasmuch as the mode can be only nondegenerate or 2-fold degenerate, the singular value decomposition should produce one singular value (for nondegenerate modes) or two singular values (for 2-fold degenerate modes) that are significantly smaller than the others. The null space vector(s) $\mathcal{B}$ of physical solutions corresponds to a propagating solution for β and characterizes the associated longitudinal electric and magnetic fields. Transverse field components (E_t and H_t) can be calculated from the longitudinal components by use of Maxwell's equations.[15]

Once we have a solution for β for a given mode, we use the transverse field components to calculate several useful physical quantities. The Poynting vector is defined as

$$S_z = \tfrac{1}{2}(E_r H_\theta^* - E_\theta H_r^*), \tag{6}$$

where the subscripts r and θ denote the field transversal components and * denotes the complex conjugate. The effective mode area (A_{eff}) is defined from the transverse electric field profile, and the usual definition is given in Ref. 1. However, in what follows (Subsection 3.B below), we introduce a modified definition for the effective mode area that is suitable for calculating the nonlinear properties of fibers that comprise different material inclusions. We also calculate the dispersion (D) of the mode, defined as in Ref. 1, from our predictions for the effective index n_{eff} over a range of wavelengths. Note that using the Sellmeier equation[1] for the refractive index of silica allows the material dispersion to be included in the calculation of the effective index of the mode from the outset. Unless otherwise stated, all calculations were performed for the fundamental mode at a wavelength of 1550 nm.

3. RESULTS

After validating the method against the previous results given in Ref. 5, we tested the method for the low-loss HF presented by scientists from NTT in Ref. 6. The fiber cladding contains 60 air holes, hexagonally packed into 4 rings. The hole diameter d was 1.7 μm, and the hole-to-hole spacing Λ was 2.8 μm (and so $d/\Lambda \sim 0.6$). The multipole method predicts an effective mode index n_{eff} of $1.422361568456178 + i2.9 \times 10^{-14}$. The predicted effective mode area is ~ 9 μm^2. Note that this value is comparable with the smallest effective mode area achieved in conventional fiber (~ 11 μm^2). We found that the predicted confinement loss for the fundamental mode at 1550 nm is $\sim 10^{-3}$ dB/km, consistent with, and significantly smaller than, the total measured loss of 1 dB/km reported in Ref. 6. Hence, even though the fabrication and material-related losses have been reduced dramatically in this fiber, they still dominate the confinement loss here.

We then applied the method to a smaller-core HF that also contained 60 air holes. The fiber is shown in Fig. 3 and in the following study is designated fiber A. The hole-to-hole spacing (Λ) and the hole diameter (d) are 1.2 and 1.08 μm, respectively ($d/\Lambda = 0.9$). Using these smaller-scale core dimensions reduces the predicted effective mode area to ~ 1.8 μm^2 (equivalent to $\gamma \sim 50\ \text{W}^{-1}\,\text{km}^{-1}$). The mode in Fig. 3 is well confined to the core region, and at these small scales an increased mode–air overlap occurs, which is reflected in the significantly lower real part of n_{eff} ($n_{\text{eff}} = 1.295844234615065 + i3.6475 \times 10^{-11}$). The predicted confinement loss for fiber A is ~ 1 dB/km, comparable with the total measured loss for the larger core NTT fiber. Despite this, it is significantly lower than losses typically reported to date in small-core HFs.

Next, we applied the multipole method to the study of small-core (highly nonlinear) HFs. The structures in the study contain 1 to 5 rings of hexagonally packed holes. We consider fibers with hole-to-hole spacings in the range $0.8\ \mu\text{m} < \Lambda < 1.8\ \mu\text{m}$ and hole diameters in the range $0.6\Lambda < d < 0.9\Lambda$, and thus the air-filling fraction of the cladding is $33\% < \text{FF} < 74\%$, where $\text{FF} = [\pi/(2\sqrt{3})](d/\Lambda)^2$. Some examples of such fibers are shown in Figs. 4(a) and 4(b). Note from Figs. 1 and 2 that this range of large air-filling fractions can be produced in practice. Within this study we also consider the extreme (theoretical) limit in which the air-filling fraction is 1, and this jacketed air-suspended rod (JASR) is shown in Fig. 4(c).

Our aim in this study is to optimize the design of highly nonlinear HFs without compromising the fiber performance in terms of confinement loss. We first present the results related to confinement loss only (Subsection 3.A) and then move on to explore the connection between loss and effective mode area (Subsection 3.B) and between effective mode area and dispersion (Subsection 3.C).

A. Confinement Losses

We calculated the confinement loss at 1550 nm for a range of fiber profiles. Consider typical HFs such as those shown in Figs. 4(a) and 4(b). We wish to understand what happens to the confinement loss as the structure dimensions are reduced. Two competing effects might be expected to occur. Scaling down the structure reduces the thickness of the silica bridges between the holes; if these bridges are small relative to the wavelength, this might be expected to decrease the leakage. Alternatively, reducing the scale decreases the distance between the core and the solid region beyond the cladding, which can cause the mode to be poorly confined.

Figure 5 (left) shows the confinement loss as a function of the hole-to-hole spacing (Λ) for different d/Λ ratios when four rings of hexagonally arranged holes are present. Regardless of the air-filling fraction, observe that confinement loss increases for the smallest-scale structures. In addition, using a bigger d/Λ (i.e., larger air holes) always reduces the loss for all values of Λ. This result is not surprising because the mode is always more tightly confined for larger air-filling fractions. Note

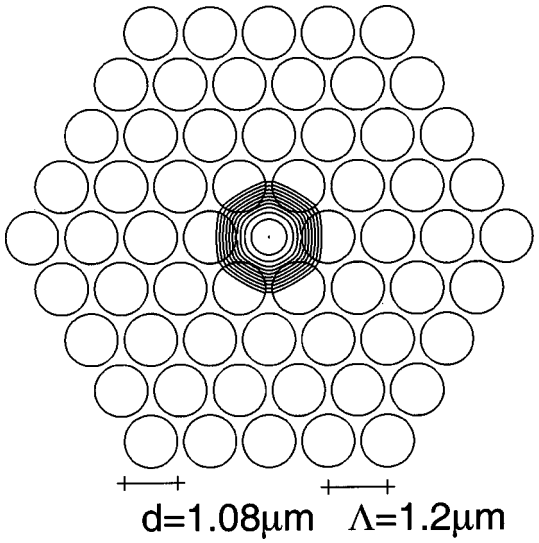

Fig. 3. Fundamental mode (2-fold degenerate) of Fiber A at 1550 nm: calculated Poynting vector (contours spaced by 2 dB).

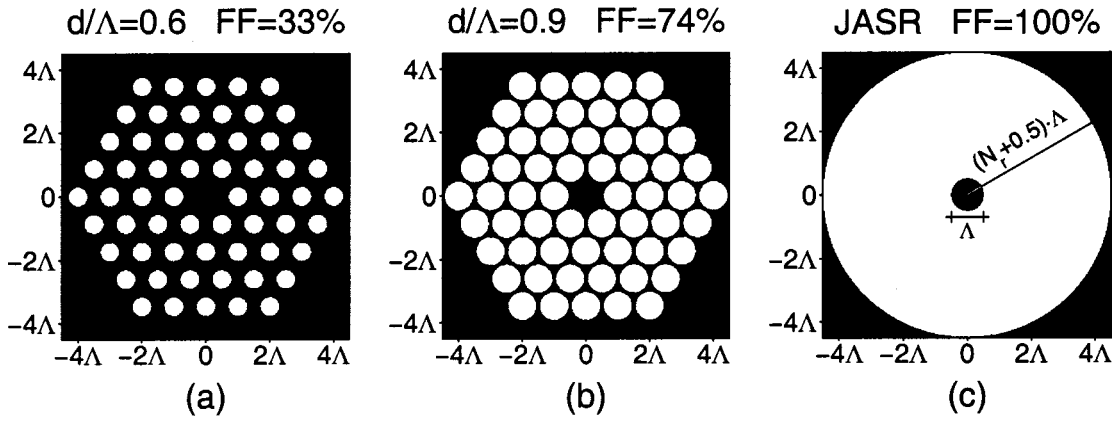

Fig. 4. Typical structures considered in this study (dark regions are silica, $n = 1.444$; white regions are air, $n = 1.0$).

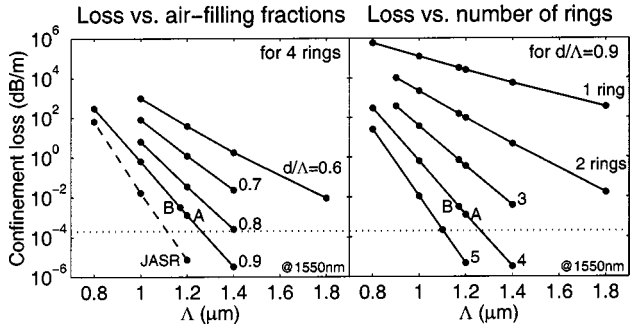

Fig. 5. Confinement loss for (left) several air-filling fractions and (right) various numbers of rings of air holes as functions of hole-to-hole spacing Λ. The dashed line at the left corresponds to JASR as defined in Fig. 4(c). Dotted horizontal line, loss of conventional fibers (0.2 dB/km). Two fibers (A and B) are labeled for reference.

that, for the smallest hole-to-hole spacings considered, the degree of improvement that results from using larger d/Λ is reduced.

To understand this trend, consider a structure in which the cladding is completely full of air, such as in Fig. 4(c). Note that the core is surrounded by a silica jacket placed a distance $(N_r + 1/2)\Lambda$ from the center (where N_r is the number of rings of the HF structure with which we wish to make a comparison). Here the extent of the air region is chosen to be equivalent to a structure with four rings of holes (i.e., $N_r = 4$). This JASR corresponds to the limit of large air-filling fractions and thus represents the best case in terms of loss for a HF with a given hole-to-hole spacing and number of rings. The dashed line in Fig. 5 represents the loss as a function of rod size for a range of JASRs. Observe that the confinement loss in the JASR is significantly larger at small rod sizes. When the JASR is scaled to small dimensions, the physical extent of the cladding region is correspondingly reduced. Hence at these small scales the benefit that one can obtain by increasing the air-filling fraction is limited because the mode can see over the finite cladding structure.

Figure 5 (right) again shows confinement loss as a function of hole-to-hole spacing (Λ), now for different numbers of rings and for a fixed air-filling fraction ($d/\Lambda = 0.9$). Regardless of the number of rings, as the core size is reduced, the loss increases. Again, not surprisingly, increasing the number of rings also always decreases the loss because the holey cladding extends over a larger region. Hence we conclude that in this regime, where the features that define the cladding are subwavelength, the main contribution to loss is due to the finite extent of the cladding structure rather than to leakage between the holes.

Note that with careful design the confinement loss can be reduced to values comparable with, or less than, the loss of conventional fibers (0.2 dB/km), which is represented by the dotted line at the bottom of each part of Fig. 5. Note that adding one extra ring to fiber A is sufficient to lower the loss below this level, from 1 to 0.01 dB/km.

B. Effective Nonlinear Mode Area

Here we identify the range of fiber profiles that lead to small effective mode areas and hence to high effective nonlinearities. The mode propagating in a HF interacts both with glass and with the air in the holes. However, air has a low nonlinearity [$n_2 \sim 3 \times 10^{-23}$ m^2/W (Ref. 16)], which is 3 orders of magnitude smaller than that of silica. The nonlinear effects in HFs are induced by the portion of the field located in the glass. To account properly for the overlap of the field with materials with different nonlinear characteristics we modified the usual definition of the effective nonlinear mode area A_{eff} given in Ref. 1 to give

$$A_{\text{eff}} = \frac{n_2\left[\int\int E_t(x, y) \cdot E_t^*(x, y)\mathrm{d}x\mathrm{d}y\right]^2}{\int\int \tilde{n}_2(x, y)[E_t(x, y) \cdot E_t^*(x, y)]^2\mathrm{d}x\mathrm{d}y}, \quad (7)$$

where $\tilde{n}_2(x, y)$ is the nonlinear-index coefficient of the material at position (x, y). This expression eliminates the contribution of any field located in the holes to the predicted mode area and hence to the effective nonlinearity. All the results given in this paper use this modified definition of effective mode area.

To ascertain the range of effective mode areas that can be achieved in a given glass material we begin by modeling the extreme case of a silica rod of diameter Λ surrounded by air [as shown in Fig. 4(c)]. As the diameter of the rod is reduced, the mode becomes increasingly more confined and the effective mode area decreases, as shown by the dashed curve in Fig. 6. Once the core size becomes significantly smaller than the optical wavelength, the rod

becomes too small to confine the light well, and the mode rapidly broadens again. Hence, as shown in the figure, there is a minimum effective mode area that, for a given optical wavelength, depends on the refractive index of the rod only. For silica, this minimum effective mode area is $\sim 1.48\ \mu m^2$, and it occurs for a rod diameter Λ of $\sim 1.2\ \mu m$.

Figure 6 also shows the effective mode area as a function of hole-to-hole spacing for a range of HFs with different air-filling fractions. These HF structures also exhibit a minimum effective mode area that is due to the same mechanism described above for the JASR. Not surprisingly, the smallest effective mode area is achieved by use of the largest air-filling fraction ($d/\Lambda = 0.9$). When $d/\Lambda = 0.9$, the minimum effective mode area value is $\sim 1.7\ \mu m^2$, only slightly larger than for the air-suspended rod. This minimum value occurs when the hole-to-hole spacing Λ is $\sim 1\ \mu m$. Observe that for smaller air-filling fractions the minimum point is shifted to larger core dimensions, which reflects the fact that for smaller air-filling fractions the index contrast between core and cladding is reduced. Note that the JASR curve crosses the HF curves at the left in Fig. 6 because the mode in the HFs can be confined somewhat by the silica bridges near the core.

Next we explore whether it is possible to design fibers with small effective mode areas and reasonably low values of confinement loss. Figure 7 shows predictions for the loss as a function of the effective mode area for structures with a fixed hole-to-hole spacing Λ of 1.2 μm and different d/Λ ratios. We chose this hole-to-hole spacing because it results in an effective mode area that is close to optimum (see Fig. 6) and the loss can be reduced below the standard fiber value by use of just five rings of air holes (see Fig. 5). Each curve in Fig. 7 corresponds to a different number of rings. Note that, for a given value of d/Λ, as the number of rings is increased, the loss decreases, as was shown above. However, observe that the effective mode area remains remarkably constant regardless of the number of rings used. Effectively, although the tails of the mode significantly influence the mode's confinement loss, their effect on the effective mode area is minimal. Indeed, when just one ring of holes is considered, the effective mode area is only slightly larger than when two or more rings are present because the mode is not well confined. For this hole-to-hole spacing (1.2 μm), increasing the air-filling fraction is always advantageous in terms of achieving both small effective mode areas and low confinement losses, regardless of the number of rings.

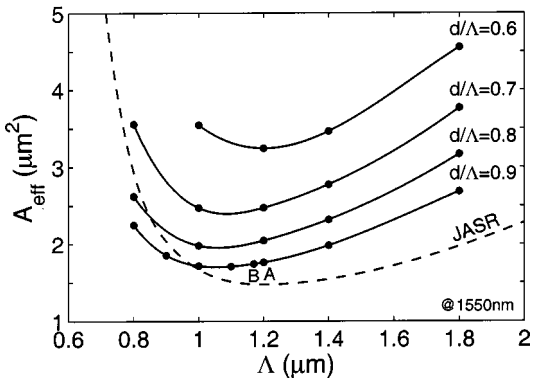

Fig. 6. Predicted effective mode area as a function of hole-to-hole spacing Λ. Dashed curve, silica JASR of diameter Λ as defined in Fig. 4(c).

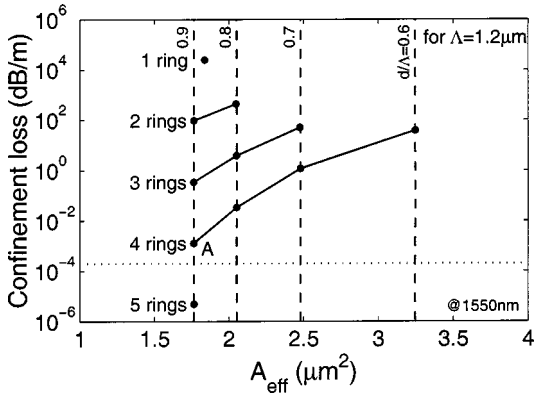

Fig. 7. Predictions of confinement loss versus effective mode area for fixed hole-to-hole spacing $\Lambda = 1.2\ \mu m$ for several numbers of rings and air-filling fractions. Dotted horizontal line, loss of conventional fibers (0.2 dB/km).

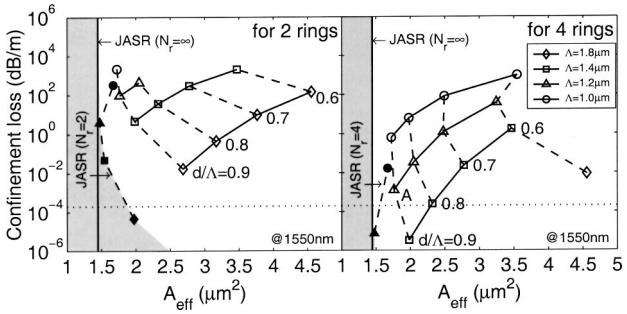

Fig. 8. Predictions of confinement loss versus effective mode area for a range of Λ and d/Λ with a fixed number of rings. Filled symbols, values for JASRs. Dotted horizontal line, loss of conventional fibers (0.2 dB/km). Shaded regions represent combinations of effective area and confinement loss that cannot be achieved with the specified number of rings.

To gain an understanding of how the trade-offs between confinement loss and effective mode area depend on the core dimensions, we begin by considering structures with two rings of holes only. The curves in Fig. 8 (left) show the loss as a function of the effective mode area for four values of the hole-to-hole spacing. In Fig. 8 the vertical lines represent the theoretical minimum effective mode area that can be achieved in an air-suspended structure (JASR with $N_r = \infty$). The smallest hole-to-hole spacings are not plotted for smaller air-filling fractions because they correspond to high loss values except when many rings of holes are used. For all hole-to-hole spacings, larger air-filling fractions not only reduce the loss but also decrease the effective mode area. The filled symbols in Fig. 8 correspond to the extreme case of a JASR, which represents the theoretical limit for both the loss and area improvements that one can obtain by moving to larger air-filling fractions. The entire shaded region at the left in Fig. 8 therefore represents combinations of effective mode area and confinement loss that cannot be achieved unless more rings of holes are added, as is confirmed in the right-hand part of Fig. 8, which shows the effect of adding two more rings of holes.

Consider the fiber shown in Fig. 8 with the relatively small air-filling fraction $d/\Lambda = 0.6$ in combination with a large core size $\Lambda = 1.8\ \mu$m. The guided mode of this fiber is filamented in shape along the silica bridges. This is the reason why the fiber has a large effective mode area compared with the other fibers considered in Fig. 8 (right). The modes of the other fibers are more nearly circular in shape.

Consider now in Fig. 8 (right) the case of a fixed hole-to-hole spacing $\Lambda = 1\ \mu$m. Observe that increasing the air-filling fraction beyond $d/\Lambda = 0.9$ does not substantially reduce the achievable effective mode area in this case. This can also be seen from Fig. 6, because when $\Lambda = 1\ \mu$m the curves for the JASR and the $d/\Lambda = 0.9$ fiber cross. This occurs because, as we have already mentioned, the presence of silica bridges near the core can help to confine the mode in this extreme regime.

Observe from Fig. 8 that, regardless of the air-filling fraction, as one moves toward smaller core dimensions there is a clear trade-off between achieving small effective mode area and low confinement loss. Such representation provide a useful practical design tool. Given an effective mode area required for a certain device and the magnitude of loss that can be tolerated (for a given device length), we can use this representation to choose a structure that minimizes the fabrication difficulties (i.e., limits the number of rings).

C. Dispersion

In Subsection 3.B we showed that it is possible to design fibers that have high effective nonlinearity and low confinement loss. We show here that by modifying the fiber profile it is possible to tailor both the magnitude and the sign of the dispersion at 1550 nm to suit a range of device applications. For example, small-core fibers with (low) normal dispersion are advantageous for optical thresholding devices (because normal dispersion reduces the impact of coherence degradation[17]), whereas anomalous dispersion allows soliton-based devices to be realized.

We calculated the dispersion for some of the structures considered in our study, concentrating on those identified in Subsection 3.B as having the most desirable properties in terms of nonlinearity and loss. In Fig. 9 the dispersion is plotted as a function of hole-to-hole spacing Λ for a fixed large air-filling fraction ($d/\Lambda = 0.9$). The dispersion curves for one, two, three, and five rings of holes are shown in the figure. Observe from Fig. 9 that the dispersion for a one-ring structure differs significantly from that of a structure with two rings of holes, particularly for small hole-to-hole spacings. In addition, observe that structures with two or more rings of holes have effectively identical dispersion values. Recall from above that the mode area is similarly independent of the number of rings of holes. We conclude that once at least two rings are used, the mode is well confined to the core, and adding further rings does not significantly affect the central part of the mode. Of course, adding further rings reduces the confinement loss, as discussed above, by acting to reduce the power in the tails of the mode distribution beyond the cladding region. Note that the difference in dispersion as a second ring is added is more marked for small hole-to-hole spacings because these structures have dimensions

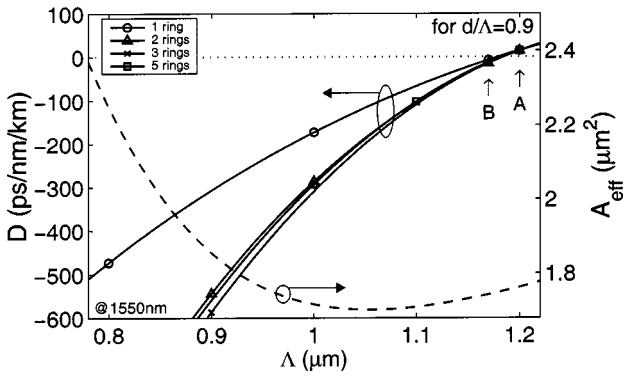

Fig. 9. Dispersion and effective mode area at a wavelength of 1550 nm as a function of hole-to-hole spacing Λ for different numbers of rings for large air-filling fraction HFs.

less than the wavelength of light, so the one-ring fiber provides relatively poorer confinement in this regime. The effective mode area as a function of the hole-to-hole spacing for two or more rings of holes and $d/\Lambda = 0.9$ is superimposed in Fig. 9 from Fig. 6 for reference purposes.

For this fixed air-filling fraction ($d/\Lambda = 0.9, FF = 74\%$), the zero-dispersion point for all curves is located near $\Lambda \sim 1.2\ \mu$m, whereas the minimum effective mode area point occurs for smaller structures, near $\Lambda \sim 1.05\ \mu$m. Figure 9 shows that we predict large normal values of dispersion for structures with $\Lambda < 1.05\ \mu$m.

For many nonlinear devices, low dispersion values are desirable, so we now concentrate on structures near the zero-dispersion wavelength. We consider one example on either side of the zero-dispersion wavelength. Fiber A (which was introduced above) and fiber B both have $d/\Lambda = 0.9$ and four rings of air holes. Fiber A has a hole-to-hole spacing of $1.2\ \mu$m, whereas B has a slightly smaller hole-to-hole spacing of $1.17\ \mu$m. Fiber A has an anomalous dispersion of +14 ps/nm/km, whereas fiber B has a normal dispersion of −14 ps/nm/km. These structures both exhibit effective mode areas of approximately $\sim 1.75\ \mu\text{m}^2$, only slightly larger than the smallest achievable mode area. Fibers A and B have similar confinement losses (of the order of ~1 dB/km). As was already stated, the addition of another ring of air holes reduces the loss to below the loss level of conventional fibers, but for the short fiber lengths typically required for nonlinear devices the four-ring loss level is tolerable. Thus small-core HF can be used to produce efficient, highly nonlinear devices characterized by near-zero, both normal and anomalous, values of dispersion.

Moving toward smaller core dimensions increases the normal dispersion; hence fiber structures within this range can be used for dispersion compensation. For example, as Fig. 9 indicates, to compensate for the dispersion of 1 km of standard SMF28 fiber [$D = +17$ ps/nm/km], just 2.8 m of a HF structure with a hole-to-hole spacing of $\Lambda \sim 0.9\ \mu$m [$D = -600$ ps/nm/km] is required. Even when five rings of holes are used, the loss for this fiber is of the order of 1 dB/m, significantly larger than for the near-zero dispersion examples given above. At least three more rings of holes are necessary to reduce the HF loss below the loss value of stan-

dard fibers. Moreover, the effective mode area for this HF is $\sim 1.86\ \mu m^2$. Such small mode areas are undesirable for a dispersion compensation device because nonlinear effects would limit the bandwidth of the data stream that can be compensated for.

The specific value of the air-filling fraction ($d/\Lambda = 0.9$) considered here was chosen for these first investigations of dispersion in small-core HFs because large air-filling fractions yield the highest effective nonlinearities. Further studies could determine whether the same trade-offs among loss, nonlinearity, and dispersion apply to structures that contain less air (i.e., $d/\Lambda < 0.9$).

4. DISCUSSION AND CONCLUSIONS

Using the multipole technique, we performed a detailed numerical study of small-core microstructured silica fibers to optimize their design for operation at 1550 nm. Structures with large air-filling fractions (and hence small effective mode areas) were considered. We found that single-material silica structures can have an effective nonlinearity more than 50 times larger than that of standard telecommunications fiber. However, the simulations indicate that these highly nonlinear fibers can suffer from significant confinement loss unless certain rules are followed when one is designing the fiber profile, as summarized here. Utilizing these rules, we can reduce the confinement loss of small-core HFs below the loss of standard fibers.

As shown in Fig. 6, the hole-to-hole spacing (Λ) can be chosen to minimize the value of the effective area of the fundamental mode (A_{eff}), and this is true regardless of the air-filling fraction. However, our loss calculations indicate that it is not always desirable to use the structures with the smallest effective mode areas because they typically exhibit higher confinement losses. A relatively modest increase in the structure scale in this small-core regime can lead to dramatic improvements in the confinement of the mode without compromising the achievable effective nonlinearity significantly. Note that one can always reduce the loss by adding more rings of holes to the fiber cladding. In the limit of core dimensions that are much smaller than the wavelength guided by the fiber, it requires many rings (>6) to ensure low-loss operation, a requirement that increases the complexity of the fabrication process.

The coupling of light into HFs with small mode areas is practically challenging compared with coupling into fibers with larger mode areas. To achieve good coupling efficiency by using free-space coupling, we require lasers with high spatial quality beams (to achieve small spot sizes) and high-NA optics. In addition, without the use of tapers or couplers the direct splicing of conventional fiber types to these fibers becomes impractical because of mode mismatch. Note that these issues are also important for highly nonlinear conventional fibers, but, because HFs can achieve smaller mode areas than conventional fiber types, the coupling of light in HF types can be more challenging.

For a complete understanding of these HF structures it is also necessary to consider the polarization properties for this range of fiber designs. Our preliminary studies indicate that, not surprisingly, polarization effects can be extreme in the small core regime. Of particular interest, the polarization extinction ratio degrades significantly when the core dimension is subwavelength, which can have a major effect on device performance. However, for the sake of brevity this issue is not discussed further here; we intend to address it in a subsequent paper.

In this study we considered only the properties of the fundamental modes of these HFs. To estimate which of the fibers in our study are single mode, we calculated the V number for a silica JASR. We found that these structures are single mode when the core diameter is smaller than $\sim 1.2\ \mu m$ and are at most few-moded for the largest dimensions considered here. HFs have an effective cladding refractive index that is always larger than 1 and so will be single mode for core sizes somewhat larger than $1.2\ \mu m$. Thus for all the device applications identified in this paper the fibers are single mode.

We also analyzed the dispersive properties of the structures to determine which designs provide the most suitable dispersion for a range of fiber device applications. We found that when the air-filling fraction is large ($d/\Lambda = 0.9$; FF = 74%), the zero-dispersion wavelength lies close to 1550 nm (within the third telecommunications window) for structures that have an effective mode area just 3% larger than the minimum achievable area. Conveniently, this promises the development of devices with low dispersion values (both anomalous and normal) with near-optimum effective nonlinearity and reasonably low confinement loss (<1 dB/km). Structures that yield the minimum effective mode area exhibit a large normal dispersion, of the order of -300 ps/nm/km. Decreasing the scale further results in even larger values of normal dispersion. As described in Subsection 3.C, such structures are of potential interest for dispersion compensation. However, as mentioned above, penalties in terms of loss occur in this regime, so making a practical device will require many rings of holes.

Interestingly, when at least two rings of holes are present, both the effective mode area and the dispersive properties of the structure are essentially independent of the number of rings. These attributes are useful because they permit quick (but remarkably accurate) calculations of the modal properties of any structure to be performed considering just two rings of holes. Once the basic properties have been calculated in this way, the confinement loss can always be reduced by addition of more holes, and indeed the loss decays exponentially with the number of rings of holes. By exploiting this fact it is possible to extrapolate the loss calculations for structures with one, two, and three rings of holes to predict the confinement loss for structures with more rings whose direct calculation by the multipole method is computationally intensive.

Our calculations indicate that the effective nonlinearity (γ) achievable in pure-silica HFs can be as high as $52\ W^{-1}\ km^{-1}$. One way to enhance the nonlinearity further is by doping the solid core. Doping with Ge, for example, can increase the value of n_2 by a factor of ~ 2. This technique was previously exploited for conventional fibers,[2] as discussed in Section 1. The preforms of most HFs fabricated to date have been made by stacking silica capillary

tubes about a solid silica rod, which ultimately forms the core. HFs with doped cores can be fabricated by replacement of the silica rod with a doped rod, and both Yb^{3+}- (Ref. 18) and Ge- (Ref. 19) doped HFs have been reported.

For glasses with higher refractive indices than silica it is possible to reach material nonlinearities that are orders of magnitude larger than that of silica. For example, the chalcogenide glass As_2S_3 has a refractive index of ~2.4 at 1550 nm and is 100 times more nonlinear than silica glass [$n_2(As_2S_3) \sim 2 \times 10^{-18}$ m^2/W].[20] Schott SF57 lead glass has a refractive index of 1.8 at 1550 nm and is 20 times more nonlinear than silica [$n_2(\mathrm{SF57}) \sim 4 \times 10^{-19}$ m^2/W].[21] Recall that for silica the theoretical lower bound for the effective mode area is ~1.45 μm^2. For the higher-index SF57 glass the minimum effective mode area is reduced to ~0.75 μm^2. Hence high-nonlinearity glasses also offer improvements in terms of mode confinement relative to silica. Note that we showed above that the minimum A_{eff} value achievable in realistic silica HFs (~1.7 μm^2) is only slightly larger than the theoretical limit, and similarly we expect that the theoretical limit will provide a useful guide to the mode areas possible in other glasses.

Conventional fibers made from As_2S_3 have been used to reduce the power levels and fiber lengths required for all-optical switching.[20] Further improvements are possible when such highly nonlinear glass is combined with the tight mode confinement offered by a HF structure. Recently, with SF57 glass, HFs with a measured effective nonlinearity γ of 550 W^{-1} km^{-1} were produced,[22,23] which is more than 500 times larger than standard silica fibers and 10 times larger than the theoretical limit for pure-silica HF structures. For this SF57 fiber the material nonlinearity (n_2) increases the value of γ by a factor of 20 relative to that of silica, whereas the small mode area ($A_{\mathrm{eff}} \sim 3$ μm^2) provides a factor-of-~28 improvement. A further factor-of-4 enhancement in nonlinearity should be achievable by use of designs that reduce the effective mode area.

We expect that the findings presented here will also facilitate the development of low-loss fibers in these glasses. Such fibers promise a route toward record effective fiber nonlinearities, paving the way to developing nonlinear fiber devices with unprecedentedly low operating powers (1–10 mW) and remarkably short device lengths (0.1–1 m).

Although in this study we have considered only pure-silica index-guiding HFs, microstructured optical fibers with periodically arranged cladding features can also guide light by making use of photonic bandgap effects. In these structures the core is formed by a defect, typically a larger air hole, in the otherwise perfect air hole lattice. In the case of an air defect, the mode can be located mostly in air. Given the low nonlinearity of air, at first sight these fibers are not particularly suitable for nonlinear applications. However, one could potentially increase the nonlinearity of this class of structure by filling the air core with a nonlinear material. The same approach could also be applied to small-core index-guiding HFs, because these fibers can have a considerable overlap between the guided mode and the air holes. For both fiber types it is important to study the effect of the refractive index of the nonlinear material that fills the holes on the guidance properties of the fiber (which could also be done with the multipole method). Here we have considered only index-guiding HFs because this technology is more mature than that of photonic bandgap fibers and because these designs naturally lead to high fiber nonlinearities.

In conclusion, index-guiding holey fibers can exhibit effective nonlinearities as high as 52 W^{-1} km^{-1}, 50 times higher than conventional fibers. We have identified the range of HF designs that lead to optimal performance in terms of mode confinement. These designs also exhibit interesting dispersive properties that make them suitable for a range of fiber device applications. However, our simulations reveal that these small-core single-material fiber designs can suffer from significant confinement loss. In this regime, confinement loss can dominate the material and processing losses, which can limit the practical application of these fibers. It is always possible to reduce the effect of this additional form of loss by introducing more air holes into the cladding region. We have shown that it is possible to envisage HFs with γ values as high as 45 W^{-1} km^{-1}, which also exhibit reasonable confinement loss levels (<0.2 dB/km) by using just four rings of holes.

ACKNOWLEDGMENTS

The authors thank Martijn de Sterke for useful discussions about the multipole method. V. Finazzi is supported by a Pirelli (Italy) studentship. T. M. Monro and D. J. Richardson are supported by Royal Society (UK) University Research Fellowships.

REFERENCES

1. G. P. Agrawal, *Nonlinear Fiber Optics* (Academic, New York, 1989).
2. T. Okuno, M. Onishi, T. Kashiwada, S. Ishikawa, and M. Nishimura, "Silica-based functional fibers with enhanced nonlinearity and their applications," IEEE J. Sel. Top. Quantum Electron. **5**, 1385–1391 (1999).
3. N. G. R. Broderick, T. M. Monro, P. J. Bennett, and D. J. Richardson, "Nonlinearity in holey optical fibers: measurement and future opportunities," Opt. Lett. **24**, 1395–1397 (1999).
4. P. Petropoulos, T. M. Monro, W. Belardi, K. Furusawa, J. H. Lee, and D. J. Richardson, "2R-regenerative all-optical switch based on a highly nonlinear holey fiber," Opt. Lett. **26**, 1233–1235 (2001).
5. T. P. White, R. C. McPhedran, C. M. de Sterke, L. C. Botten, and M. J. Steel, "Confinement losses in microstructured optical fibers," Opt. Lett. **26**, 1660–1662 (2001).
6. K. Tajima, K. Nakajima, K. Kurokawa, N. Yoshizawa, and M. Ohashi, "Low-loss photonic crystal fibers," in *Optical Fiber Communication*, Vol. 70 of OSA Trends in Optics and Photonics Series (Optical Society of America, Washington, D.C., 2002), pp. 523–524.
7. V. Finazzi, T. M. Monro, and D. J. Richardson, "Confinement loss in highly nonlinear holey optical fibers," in *Optical Fiber Communication*, Vol. 70 of OSA Trends in Optics and Photonics Series (Optical Society of America, Washington, D.C., 2002), pp. 524–525.

8. Z. Yusoff, J. H. Lee, W. Belardi, T. M. Monro, P. C. Teh, and D. J. Richardson, "Raman effects in a highly nonlinear holey fiber: amplification and modulation," Opt. Lett. **27**, 424–426 (2002).
9. T. P. White, R. C. McPhedran, L. C. Botten, G. H. Smith, and C. M. de Sterke, "Calculations of air-guided modes in photonic crystal fibers using the multipole method," Opt. Express **9**, 721–732 (2001), http://www.opticsexpress.org.
10. W. Wijngaard, "Guided normal modes of two parallel circular dielectric rods," J. Opt. Soc. Am. **63**, 944–949 (1973).
11. M. Abramowitz and I. A. Stegun, *Handbook of Mathematical Functions* (Dover, New York, 1965).
12. Lord Rayleigh, "On the influence of obstacles arranged in rectangular order upon the properties of a medium," Phil. Mag. **34**, 481–502 (1892).
13. P. R. McIsaac, "Symmetry-induced modal characteristics of uniform waveguides. I. Summary of results," IEEE Trans. Microwave Theory Tech. **MTT-23**, 421–429 (1975).
14. M. J. Steel, T. P. White, C. M. de Sterke, R. C. McPhedran, and L. C. Botten, "Symmetry and degeneracy in microstructured optical fibers," Opt. Lett. **26**, 488–490 (2001).
15. A. W. Snyder and J. D. Love, in *Optical Waveguide Theory* (Chapman & Hall, London, 1995), Chap. 30, p. 593.
16. D. N. Nikogosyan, *Optical and Laser-Related Materials* (Wiley, Chichester, UK, 1997).
17. N. Nakazawa, H. Kubota, and K. Tamura, "Random evolution and coherence degradation of a high-order optical soliton train in the presence of noise," Opt. Lett. **24**, 318–320 (1999).
18. K. Furusawa, T. M. Monro, P. Petropoulos, and D. J. Richardson, "Modelocked laser based on ytterbium doped holey fibre," Electron. Lett. **37**, 560–561 (2001).
19. B. J. Eggleton, P. S. Westbrook, R. S. Windeler, S. Spälter, and T. A. Strasser, "Grating resonances in air–silica microstructured optical fibers," Opt. Lett. **24**, 1460–1462 (1999).
20. M. Asobe, "Nonlinear optical properties of chalcogenide glass fibers and their application to all-optical switching," Opt. Fiber Technol. **3**, 142–148 (1997).
21. S. R. Friberg and P. W. Smith, "Nonlinear optical-glasses for ultrafast optical switches," IEEE J. Quantum Electron. **23**, 2089–2094 (1987).
22. T. M. Monro, K. M. Kiang, J. H. Lee, K. Frampton, Z. Yusoff, R. Moore, J. Tucknott, D. W. Hewak, H. N. Rutt, and D. J. Richardson "High nonlinear extruded single-mode holey optical fibers," in *Optical Fiber Communication*, Vol. 70 of OSA Trends in Optics and Photonics Series (Optical Society of America, Washington, D.C., 2002), 315–317.
23. K. M. Kiang, K. Frampton, T. M. Monro, R. Moore, J. Tucknott, D. W. Hewak, and D. J. Richardson, "Extruded single-mode non-silica glass holey optical fibers," Electron. Lett. **38**, 546–547 (2002).